

고분자 태양전지용 DPP와 Furan 기반 단분자 어셉터의 CN 치환기 효과

임은희[†]

경기대학교 화학과

(2020년 3월 25일 접수, 2020년 4월 13일 수정, 2020년 4월 14일 채택)

Influence of CN Substitution on DPP-furan-based Small-molecule Acceptors for Polymer Solar Cells

Eunhee Lim[†]

Department of Chemistry, Kyonggi University, 154-42 Gwanggyosan-ro, Yeongtong-gu, Suwon 16227, Korea

(Received March 25, 2020; Revised April 13, 2020; Accepted April 14, 2020)

초록: 본 연구에서는, 스즈키 짝지음 반응을 이용하여 *p*- 및 *o*-DPP-F-PhCN의 두 단분자를 합성하여 고분자 태양전지의 비풀러렌계 어셉터로 사용하였다. 치환기의 위치 및 퓨란 효과에 따른 단분자의 물리적 특성 변화를 살펴보았다. 퓨란 그룹의 도입으로 단분자는 더 높은 상전이 온도와 HOMO 및 LUMO 준위를 나타내었다. *o*-치환 역시 분자의 에너지 준위를 높게 함으로써, *o*-DPP-F-PhCN의 에너지 준위가 가장 높게 나타났다. 상대적으로 강하고 장파장 이동된 UV-vis 흡수는 *o*-DPP-F-PhCN의 강한 분자 응집을 나타낸다. P3HT와 DPP-F-PhCN들을 각각 고분자 도너와 비풀러렌계 어셉터로 사용한 고분자 태양전지를 제작하였고, 두 DPP-F-PhCN이 유사한 효율을 나타내었다. *o*-DPP-F-PhCN의 강한 응집 거동은 외부양자효율에 유리하였으나, 향상된 오비탈 상호작용에 따른 안정화된 LUMO 준위로 인해 상대적으로 낮은 개방전압 값을 나타내었다.

Abstract: In this study, two small-molecules, *p*- and *o*-DPP-F-PhCN, were synthesized via a Suzuki coupling reaction and used as nonfullerene acceptors (NFAs) for poly(3-hexylthiophene) (P3HT)-based polymer solar cells (PSCs). The physical properties of the molecules were examined in terms of the substituent position and the effect of the furan moiety. The introduction of a furan moiety resulted in higher phase-transition temperatures and higher-lying molecular orbital energy levels of the molecules. Substitution at the ortho position also elevated the energy levels of the molecules, resulting in the highest-lying values for *o*-DPP-F-PhCN. A relatively enhanced and red-shifted UV-vis absorption of *o*-DPP-F-PhCN indicated its stronger molecular aggregation. PSCs based on two DPP-F-PhCNs exhibited similar device efficiencies. The stronger aggregation behavior of *o*-DPP-F-PhCN led to a device with a better external quantum efficiency profile; however, the enhanced orbital interactions and resulting stabilized the lowest unoccupied molecular orbital level of *o*-DPP-F-PhCN led to a relatively low open-circuit voltage.

Keywords: polymer solar cells, organic photovoltaic cells.

Introduction

Recently, nonfullerene acceptors (NFAs) have been spotlighted as replacements for the traditional fullerene acceptors in polymer solar cells (PSCs). Most successful examples are acceptor-donor-acceptor (A-D-A)-type small-molecule NFAs composed of ladder-type electron-donating cores (e.g., indacenodithiophene or indacenodithieno[3,2-*b*]thiophene) and

electron-withdrawing dye end groups (e.g., rhodanine (RH) or 1,1-dicyanomethylene-3-indanone).^{1,2} Continuous and intensive efforts toward the development of various A-D-A-type NFAs has opened a path to the development of high-efficiency PSCs. A certified power conversion efficiency (PCE) of 17.29% was achieved in 2018 using a solution-processed tandem PSC in which two NFAs (F-M and CO₈DFIC) were used in the rear (PBDB-T:F-M) and front (PTB7-Th:CO₈DFIC:PC₇₁BM) sub-cells, respectively, resulting in high external quantum efficiency (EQE) responses greater than 70% in the whole UV-vis and infrared absorption ranges covering wavelengths as long as 1000 nm.³ More recently, a high PCE of 17.0% was also

[†]To whom correspondence should be addressed.
ehlim@kyonggi.ac.kr, ORCID[®]0000-0002-2321-7072
©2020 The Polymer Society of Korea. All rights reserved.

demonstrated in single-junction PSCs composed of PBDBTF and BTP-4Cl-12 as a polymer donor and an NFA, respectively, through side-chain engineering.⁴ However, most of the reported high-efficiency NFAs have been composed of ladder-type aromatic rings with extended π -conjugation, which requires multiple synthesis steps and inevitably involves high synthesis costs; thus, this approach is not applicable to the future commercialization of PSCs. Consequently, NFAs based on non-fused core systems have recently been attracting increasing interest.^{1,5-8}

Side-chain engineering (i.e., length and bulkiness) and/or substituent effects (i.e., electron-donating or -withdrawing groups) have been explored to fine-tune the physical properties of organic semiconducting materials, including their solubility and molecular aggregation behavior.^{1,4,9} The position of side chains and substituents can also affect the physical properties of the resultant molecules. For example, Janssen *et al.* systematically investigated the influence of the position of the alkyl side chain on the photovoltaic properties of 2,5-diketopyrrolo[3,4-*c*]pyrrole (DPP)-based small molecules¹⁰ and found that the morphology and crystallization of the small molecules varied according to the side-chain position. In addition, our group has reported the effect of hexyl or cyanide (CN) groups on the photovoltaic properties of benzothiadiazole–thiophene-based small molecules (2-, 3-, and 4-hexyl-substituted DH5TBs)¹¹ or DPP–thiophene-based small molecules (*p*-, *m*-, and *o*-DPP-PhCNs), respectively.¹²

In the present work, we developed two small molecules, *p*- and *o*-DPP-F-PhCN, in which electron-withdrawing CN groups were introduced at different positions (para and ortho, respectively) on the phenyl end groups, and observed their different molecular packing behaviors and photovoltaic properties. In particular, we used differential scanning calorimetry (DSC), UV–vis absorption spectroscopy, and cyclic voltammetry (CV) measurements to systematically investigate how the introduction of a furan moiety altered the physical properties of the molecules.

Experimental

Materials. Tris(dibenzylideneacetone)dipalladium(0) ($\text{Pd}_2(\text{dba})_3$), 4-cyanophenylboronic acid pinacol ester, tri-*tert*-butylphosphonium tetrafluoroborate ($\text{P}(t\text{-Bu})_3 \times \text{HBF}_4$), and potassium phosphate tribasic (K_3PO_4) were purchased from Sigma Aldrich. 2-Cyanophenylboronic acid pinacol ester was purchased from Alfa Aesar. All chemicals were used without fur-

ther purification, and all reactions were performed under a nitrogen atmosphere with anhydrous solvents.

Synthesis. DPP-F-Br was synthesized according to the literature.^{13,14} *p*- and *o*-DPP-F-PhCN were synthesized using a palladium-catalyzed Suzuki coupling reaction between DPP-F-Br and boronic esters, 4- and 2-cyanophenylboronic acid pinacol ester, respectively.^{12,15}

Synthesis of *p*-DPP-F-PhCN: A degassed aqueous solution (1.3 mL) of K_3PO_4 (0.40 g, 1.9 mmol) was added to 12 mL of degassed tetrahydrofuran (THF) solution of DPP-F-Br (0.40 g, 0.62 mmol), $\text{Pd}_2(\text{dba})_3$ (0.016 g, 0.017 mmol), $\text{P}(t\text{-Bu})_3 \times \text{HBF}_4$ (0.010 g, 0.033 mmol), and 4-cyanophenylboronic acid pinacol ester (0.45 g, 2.5 mmol) under N_2 atmosphere. After the mixture was heated to 80 °C for 12 h, the reaction was cooled to room temperature. The mixture was extracted with dichloromethane and water. The collected organic layer was dried over MgSO_4 . After removing the solvent under reduced pressure, the crude product was purified by column chromatography on silica using dichloromethane as the eluent, to afford *p*-DPP-F-PhCN as a dark green powder (0.37 g, yield 86%). ¹H NMR (CDCl_3 , 400 MHz): δ (ppm) 8.43 (*d*, 2H), 7.85 (*d*, 4H), 7.74 (*d*, 4H), 7.12 (*d*, 2H), 4.16 (*m*, 4H), 1.89 (*m*, 2H), 1.23–1.46 (*m*, 16H), 0.90 (*t*, 6H), 0.83 (*t*, 6H). ¹³C NMR (CDCl_3 , 100MHz): δ (ppm) 161.03, 154.58, 145.26, 133.16, 133.06, 132.85, 124.71, 122.46, 118.50, 111.88, 111.83, 108.10, 46.70, 39.48, 30.37, 28.54, 23.59, 23.16, 14.03, 10.56. Anal. calcd for $\text{C}_{44}\text{H}_{46}\text{N}_4\text{O}_4$: C, 76.05; H, 6.67; N, 8.06; O, 9.21. Found: C, 76.22; H, 6.72; N, 8.10.

Synthesis of *o*-DPP-F-PhCN: *o*-DPP-F-PhCN was prepared in the same manner as *p*-DPP-F-PhCN using a degassed aqueous solution (1.1 mL) of K_3PO_4 (0.33 g, 1.6 mmol), 9.4 mL of degassed THF solution of DPP-F-Br (0.33 g, 0.51 mmol), $\text{Pd}_2(\text{dba})_3$ (0.013 g, 0.014 mmol), $\text{P}(t\text{-Bu})_3 \times \text{HBF}_4$ (8.0 mg, 0.027 mmol), and 2-cyanophenylboronic acid pinacol ester (0.47 g, 2.04 mmol), to afford *o*-DPP-F-PhCN as a purple powder (0.31 g, yield 89%). ¹H NMR (CDCl_3 , 400 MHz): δ (ppm) 8.35 (*d*, 2H), 7.94 (*d*, 2H), 7.72 (*dd*, 2H), 7.64 (*td*, 2H), 7.53 (*d*, 2H), 7.39 (*td*, 2H), 4.11 (*m*, 4H), 1.80 (*m*, 2H), 1.13–1.36 (*m*, 16H), 0.81 (*t*, 6H), 0.73 (*t*, 6H). ¹³C NMR (CDCl_3 , 100 MHz): δ (ppm) 160.95, 152.28, 144.81, 134.55, 133.16, 131.72, 128.54, 126.53, 122.22, 118.55, 113.94, 108.15, 107.83, 46.48, 39.51, 30.34, 28.54, 23.57, 23.15, 14.02, 10.58. Anal. calcd for $\text{C}_{44}\text{H}_{46}\text{N}_4\text{O}_4$: C, 76.05; H, 6.67; N, 8.06; O, 9.21. Found: C, 76.56; H, 6.74; N, 8.22.

Physical Measurements. NMR spectra were recorded on a Bruker AVANCE II 400 spectrometer. Elemental analyses

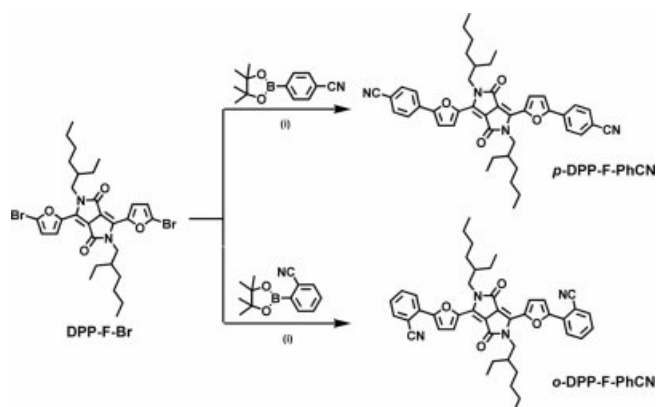
were performed with a Flash EA 1112 series from Thermo Electron Corporation. Thermogravimetric analysis (TGA) and DSC were performed on a TGA/DSC 1 thermogravimetric analyzer from Mettler-Toledo Inc. under a nitrogen atmosphere at a heating or cooling rate of 10 °C/min. UV-vis spectra were obtained using a Shimadzu UV-2550 spectrometer. The electrochemical properties of the small molecules were studied by CV with a BAS 100B electrochemical analyzer. The films were prepared by dip-coating the small molecule solution onto a Pt working electrode. Detailed experimental methods are given in previous reports.¹²

Fabrication of PSCs. In this study, we fabricated the devices with the structures of ITO/PEDOT:PSS/poly(3-hexylthiophene) (P3HT):acceptor/LiF/Al. The ITO-coated glass substrates were pre-treated in a UV-ozone oven for 15 min. A layer of PEDOT:PSS (~30 nm) was spin-coated on top of the ITO-coated glass substrates. The active layer was spin-cast at 3000 rpm from a chloroform solution of donor and acceptor with a total solids concentration of 15 mg mL⁻¹. The average thickness of the active layers (~100 nm) was measured with an Alpha-Step IQ surface profiler. A LiF (~0.5 nm) and Al (~100 nm) layer were directly deposited on the active layer under a vacuum of ~10⁻⁶ Torr. The effective area of all devices was measured to be 9 mm². The current-density vs. voltage ($J-V$) and EQE curves were recorded using the same methods described in our previous report.¹²

Results and Discussion

Synthesis and Thermal Properties. The two small molecules *p*- and *o*-DPP-F-PhCN were synthesized via a Suzuki coupling reaction between the dibromides of a DPP-furan-based core (DPP-F-Br) and two corresponding boronic esters (4- and 2-cyanophenylboronic acid pinacol ester, respectively) using a Pd catalyst (Scheme 1). The synthesized small molecules were successfully characterized by ¹H- and ¹³C NMR spectroscopy (Figures S1–S2) and elemental analysis.

The thermal characteristics of the small molecules are sum-



Scheme 1. Synthetic procedure for DPP-F-PhCNs. (i) Pd₂(dba)₃, P(*t*-Bu)₃ × HBF₄, K₃PO₄, THF, H₂O, 80 °C, 12 h.

marized in Table 1. The two compounds were thermally stable, showing 5% weight losses upon being heated to 380 °C in TGA analysis (Figure 1(a)). The phase-transition temperatures were measured by DSC (Figure 1(b)). The melting temperatures (T_m) of *p*- and *o*-DPP-F-PhCN were 300 and 206 °C, respectively. We likewise observed a higher T_m for the para-substituted analogue in our previous work with DPP-PhCNs,¹² where *p*-DPP-PhCN exhibited a higher T_m (251 °C) than *o*-DPP-PhCN (T_m = 187 °C). In addition, the introduction of furan resulted in higher T_m values; for example, the T_m of *p*-DPP-F-PhCN (300 °C) was higher than that of the thiophene analogue *p*-DPP-PhCN (T_m = 251 °C) by approximately 50 °C. Notably, *o*-DPP-F-PhCN exhibited an enthalpy change (ΔH_m = -100 J/g) more negative than that of *p*-DPP-F-PhCN (-85 J/g), reflecting the relatively better crystallinity of *o*-DPP-F-PhCN. By contrast, in our previous work on DPP-PhCNs, *p*-DPP-PhCN exhibited a ΔH_m (-111 J/g) more negative than that of *o*-DPP-PhCN (-86 J/g).¹²

Optical and Electrochemical Properties. The UV-vis absorption spectra of *p*- and *o*-DPP-F-PhCN in the solution and film states are shown in Figure 2. In the solution state, *p*- and *o*-DPP-F-PhCN exhibited similar UV-vis absorption profiles; however, the absorption maximum of *p*-DPP-F-PhCN

Table 1. Physical Properties of DPP-F-PhCNs

Acceptor	T_{5d}^a (°C)	T_m (°C)	ΔH_m (J/g)	λ_{max} (nm)		$E_{g,opt}^b$ (eV)	HOMO _{elec} (eV)	LUMO _{opt} ^c (eV)
				soln	film			
<i>p</i> -DPP-F-PhCN	397	300	-85	610	570	1.80	-5.37	-3.57
<i>o</i> -DPP-F-PhCN	384	206	-100	599	638	1.86	-5.32	-3.46

^a T_{5d} are the decomposition temperatures showing 5% of the weight losses. ^b $E_{g,opt}$ were calculated from the onset of absorption spectra in film ($E_{g,opt} = 1240/\lambda_{onset}$ (eV)). ^cLUMO_{opt} were estimated using HOMO_{elec} levels and $E_{g,opt}$ (LUMO_{opt} = HOMO_{elec} + $E_{g,opt}$).

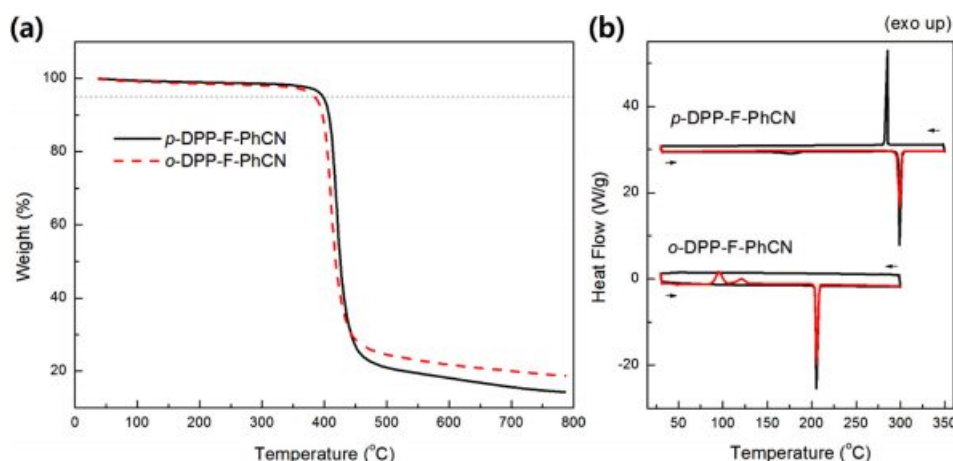


Figure 1. (a) TGA; (b) DSC curves of DPP-F-PhCNs.

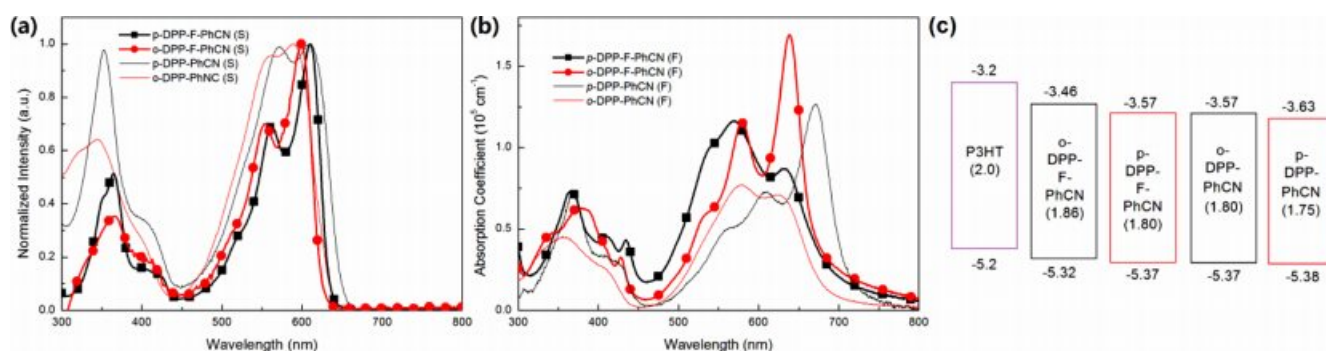


Figure 2. UV absorption spectra in (a) solution; (b) films; (c) energy diagram of DPP-F-PhCNs and DPP-PhCNs. The values in parentheses are $E_{g,opt}$, which were calculated from the absorption onset of the small molecule films ($E_g = 1240/\lambda_{onset}$ (eV)); the LUMO_{opt} levels were calculated from the HOMO_{elec} and $E_{g,opt}$ values.

($\lambda_{max} = 601$ nm) was slightly red-shifted compared with that of *o*-DPP-F-PhCN ($\lambda_{max} = 599$ nm), in agreement with the trend observed for DPP-PhCNs. That is, the conjugation in the *para*-substituted analogue might be slightly longer than that in the *ortho*-substituted analogue. In the spectra of *p*- and *o*-DPP-F-PhCN films, the absorption peaks were broader than those in the spectra of the solution state samples. In particular, as shown in Figure S3, the absorption maximum of *o*-DPP-F-PhCN was dramatically red-shifted by approximately 40 nm from its position in the solution-state spectrum ($\lambda_{max} = 599$ nm) to that in the film-state spectrum ($\lambda_{max} = 638$ nm). We observed a similar phenomenon in our previous experiments with *p*-DPP-PhCN (but not *o*-DPP-PhCN),¹² where the greater red-shift in the absorption of *p*-DPP-PhCN ($\lambda_{max} = 670$ nm) was explained by its high degree of molecular aggregation. Interestingly, the film aggregation behavior and absorption profiles of the small molecules used in the present study were con-

trolled by the nature of the π -bridge (i.e., thiophene vs. furan) as well as by the position of the substituents (i.e., *para* vs. *ortho*). In addition, the optical bandgaps ($E_{g,opt}$) of the small molecules were calculated to be 1.80 and 1.86 eV for *p*- and *o*-DPP-F-PhCN, respectively, using the following equation: $E_{g,opt} = 1240/\lambda_{onset}$ (eV), where λ_{onset} is the wavelength of the absorption onset of the small molecule films.

The highest occupied molecular orbital (HOMO_{elec}) and the lowest unoccupied molecular orbital (LUMO_{elec}) energy levels were estimated from the CV, as shown in Figure 3, using the following equations: HOMO_{elec} = ($E_{onset,ox} - E_{1/2,ferrocene} + 4.8$) eV and LUMO_{elec} = ($E_{onset,red} - E_{1/2,ferrocene} + 4.8$) eV, where $E_{onset,ox}$ and $E_{onset,red}$ are the onset potentials of oxidation and reduction, respectively, assuming that the energy level of ferrocene (Fc) is 4.8 eV below the vacuum level.^{6,16-18} The position of the substituent (CN) affects the energy levels of the small molecules: *para*-substitution resulted in relatively low-lying HOMO_{elec}/

LUMO_{elec} energy levels for *p*-DPP-F-PhCN (-5.37/-3.57 eV) relative to those of *o*-DPP-F-PhCN (-5.32/-3.53 eV). Both small molecules have sufficient HOMO and LUMO offsets with respect to the P3HT polymer used as a donor in PSC fabrication, enabling not only electron transfer from the P3HT to the small molecules but also hole transfer from the small molecules to the P3HT (*i.e.*, Channel II charge generation).¹²

Figure 2(c) compares the energy levels of DPP-F-PhCNs with those of the DPP-PhCN thiophene analogues to illustrate how the incorporation of the furan moiety affects the electrochemical properties of the small molecules; the optical LUMO energy levels (LUMO_{opt}) were estimated from the HOMO_{elec} energy levels and the optical $E_{g, opt}$ (LUMO_{opt} = HOMO_{elec} + $E_{g, opt}$). The furan substitution elevated both the HOMO and LUMO energy levels of the small molecules, where it exerted a slightly stronger effect on the LUMO levels than on the HOMO levels.

Photovoltaic Performances. PSCs were fabricated with the configuration ITO/PEDOT:PSS/active layer/LiF/Al. Both small molecules could act as acceptors when combined with regioregular P3HT as a polymer donor because of the sufficient HOMO and LUMO offsets between the donor and acceptors, as previously discussed (Figure 3). Moderate PCEs of ~0.3% were obtained with the P3HT:DPP-F-PhCN devices. The $J-V$ and EQE curves were recorded in air under white-light AM 1.5G illumination (100 mW cm⁻²) and are shown in Figure 4. The active area (*i.e.*, the aperture area in a mask) was defined as 9 mm². The optimized photovoltaic properties are summarized in Table 2.

The short-circuit current density (J_{sc}) values were found to be similar between the devices with the two DPP-F-PhCNs as well as between the devices with the two DPP-PhCNs. The maximum EQE intensities of the DPP-F-PhCN-based devices were also similar; however, we note that the EQE profile of the

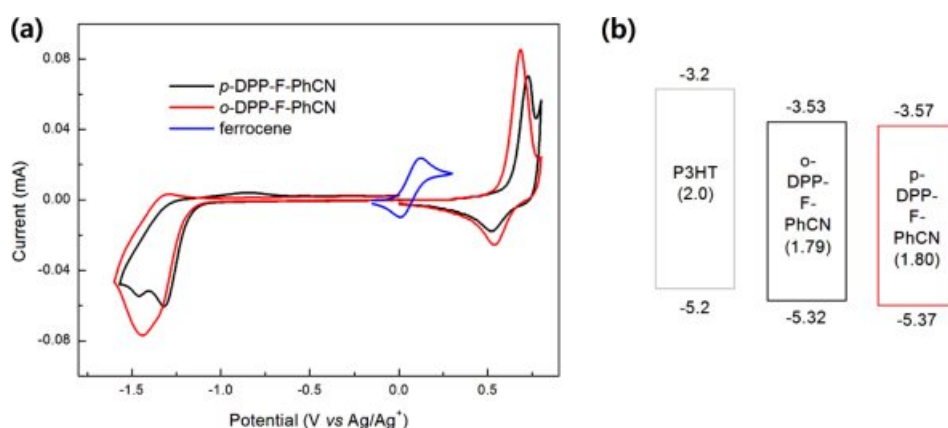


Figure 3. (a) CV; (b) energy diagrams of DPP-F-PhCNs. The values in parentheses are the electrochemical energy bandgaps ($E_{g, elec}$) calculated from the HOMO_{elec} and LUMO_{elec} energy levels in CV measurements.

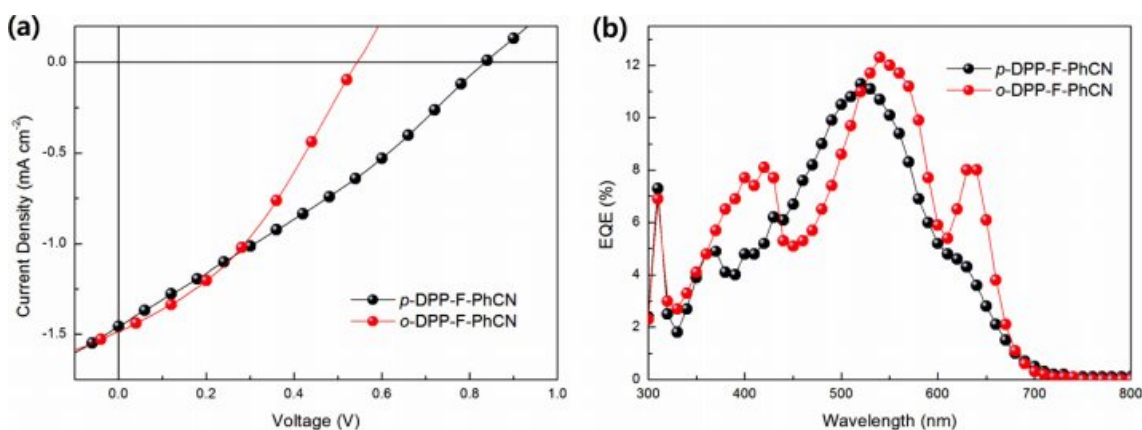


Figure 4. (a) $J-V$ curves; (b) EQE responses of P3HT:acceptor devices.

Table 2. Optimized Photovoltaic Performances of P3HT: Acceptor Devices^a

	V_{OC} (V)	J_{SC} (mA/cm ²)	FF (%)	PCE (%)
<i>p</i> -DPP-F-PhCN	0.83	1.46	29	0.36
<i>o</i> -DPP-F-PhCN	0.54	1.48	36	0.29
<i>p</i> -DPP-PhCN ^b	0.56	1.64	50	0.47
<i>o</i> -DPP-PhCN ^b	1.09	1.19	35	0.46

^aThe device architecture is ITO/PEDOT:PSS/P3HT:acceptor (1:1, w/w)/LiF/Al. The active layers were prepared by spin-coating of a chloroform solution of donor and acceptor, and the devices were annealed for 10 min. ^bData taken from ref [12].

o-DPP-F-PhCN-based device was red-shifted relative to that of the *p*-DPP-F-PhCN-based device, consistent with the absorption profiles of the two DPP-F-PhCN films. In particular, the additional sharp EQE response at 635 nm coincides with the absorption maximum of the *o*-DPP-F-PhCN film ($\lambda_{max} = 638$ nm). Interestingly, the EQE and absorption profiles of *o*-DPP-F-PhCN are similar to those of *p*-DPP-PhCN, not those of *o*-DPP-PhCN. Among the thiophene analogues of DPP-PhCNs, *p*-DPP-PhCN exhibited the highest degree of molecular aggregation, whereas the introduction of a furan moiety altered the aggregation behavior of the molecules and the *ortho*-substitution resulted in greater molecular aggregation and a red-shift of the absorption maximum, leading to the additional EQE response at long wavelengths.

The slightly higher PCE of *p*-DPP-F-PhCN originated from its higher open-circuit voltage (V_{OC}) of 0.83 V compared with that of *o*-DPP-F-PhCN ($V_{OC} = 0.54$ V). This result is inconsistent with the general understanding that the V_{OC} values of the devices generally depend on the energy difference between the HOMO level of the donor and the LUMO level of the acceptor.¹⁹ For a given HOMO level of the donor, *o*-DPP-F-PhCN, which has a higher LUMO level than *p*-DPP-F-PhCN, is expected to result in a device with a higher V_{OC} ; however, the V_{OC} of the *o*-DPP-F-PhCN-based device ($V_{OC} = 0.54$ V) was lower than expected. This result is attributable to the strong aggregation of *o*-DPP-F-PhCN, as confirmed by its absorption spectrum (Figure 2) and high ΔH_m , where the enhanced orbital interactions could destabilize/stabilize the HOMO/LUMO levels of the aggregates.¹² Further improvements of photovoltaic properties could be achieved by optimizing device fabrication conditions and introducing a low bandgap polymer donor or a third component for ternary cells.)

Conclusions

The *p*- and *o*-DPP-F-PhCN were synthesized for use as NFAs in PSCs. The optical and electrochemical properties of the small molecules varied according to both the substituent position and the furan effect. Among the DPP-F-PhCNs and DPP-PhCNs, the highest-lying HOMO and LUMO levels were observed in *o*-DPP-F-PhCN because of both the furan introduction and the *ortho*-substitution. The relatively red-shifted and enhanced λ_{max} in the UV-vis absorption spectra and greater enthalpy change of *o*-DPP-F-PhCN relative to that of *p*-DPP-F-PhCN indicated stronger molecular aggregation behavior of *o*-DPP-F-PhCN, leading to the observed EQE response at long wavelengths. Such strong aggregation of *o*-DPP-F-PhCN resulted in a relatively low V_{OC} value in the device despite its highest-lying LUMO level, which can be explained by the enhanced orbital interactions and thus stabilized LUMO level of *o*-DPP-F-PhCN.

Acknowledgments: This work was supported by Kyonggi University Research Grant 2017.

Supporting Information: Information is available regarding ¹H and ¹³C NMR spectra, UV-vis absorption, and all-OSC characterization. The materials are available via the Internet at <http://journal.polymer-korea.or.kr>.

References

1. R. D. Maduwu, H. C. Jin, and J. H. Kim, *Macromol. Res.*, **27**, 1261 (2019).
2. M. H. Hoang, G. E. Park, D. L. Phan, T. T. Ngo, T. V. Nguyen, C. G. Park, M. J. Cho, and D. H. Choi, *Macromol. Res.*, **26**, 844 (2018).
3. L. Meng, Y. Zhang, X. Wan, C. Li, X. Zhang, Y. Wang, X. Ke, Z. Xiao, L. Ding, R. Xia, H.-L. Yip, Y. Cao, and Y. Chen, *Science*, **361**, 1094 (2018).
4. Y. Cui, H. Yao, L. Hong, T. Zhang, Y. Tang, B. Lin, K. Xian, B. Gao, C. An, P. Bi, W. Ma, and J. Hou, *Nat. Sci. Rev.*, nzw200 (2019).
5. S. Pang, X. Zhou, S. Zhang, H. Tang, S. Dhakal, X. Gu, C. Duan, F. Huang, and Y. Cao, *ACS Appl. Mater. Interf.*, **12**, 16531 (2020).
6. T. Lee, Y. Eom, C. E. Song, I. H. Jung, D. Kim, S. K. Lee, W. S. Shin, and E. Lim, *Adv. Energy Mater.*, **9**, 1804021 (2019).
7. X. Li, Y. Wang, Q. Zhu, X. Guo, W. Ma, X. Ou, M. Zhang, and Y. Li, *J. Mater. Chem. A*, **7**, 3682 (2019).
8. Z.-P. Yu, Z.-X. Liu, F.-X. Chen, R. Qin, T.-K. Lau, J.-L. Yin, X. Kong, X. Lu, M. Shi, C.-Z. Li, and H. Chen, *Nat. Commun.*, **10**, 2152 (2019).

9. T. Liu, X. Pan, X. Meng, Y. Liu, D. Wei, W. Ma, L. Huo, X. Sun, T. H. Lee, M. Huang, H. Choi, J. Y. Kim, W. C. H. Choy, and Y. Sun, *Adv. Mater.*, **29**, 1604251 (2017).
10. V. S. Gevaerts, E. M. Herzig, M. Kirkus, K. H. Hendriks, M. M. Wienk, J. Perlich, P. Müller-Buschbaum, and R. A. J. Janssen, *Chem. Mater.*, **26**, 916 (2013).
11. E. Lim, S. Lee, K. K. Lee, I.-N. Kang, S.-J. Moon, H.-Y. Kong, and H. E. Katz, *Sol. Energ. Mat. Sol. C*, **107**, 165 (2012).
12. Y. Kim, C. E. Song, E. J. Ko, D. Kim, S. J. Moon, and E. Lim, *RSC Adv.*, **5**, 4811 (2015).
13. C. H. Woo, P. M. Beaujuge, T. W. Holcombe, O. P. Lee, and J. M. J. Fréchet, *J. Am. Chem. Soc.*, **132**, 15547 (2010).
14. P. Sonar, S. P. Singh, E. L. Williams, Y. Li, M. S. Soh, and A. Dodabalapur, *J. Mater. Chem.*, **22**, 4425 (2012).
15. H. Bürckstümmer, A. Weissenstein, D. Bialas, and F. Würthner, *J. Org. Chem.*, **76**, 2426 (2011).
16. Y. Eom and E. Lim, *Polym. Korea*, **39**, 986 (2015).
17. D. Liu, B. Kan, X. Ke, N. Zheng, Z. Xie, D. Lu, and Y. Liu, *Adv. Energy Mater.*, **8**, 1801618 (2018).
18. M. Zhang, Z. Xiao, W. Gao, Q. Liu, K. Jin, W. Wang, Y. Mi, Q. An, X. Ma, X. Liu, C. Yang, L. Ding, and F. Zhang, *Adv. Energy Mater.*, **8**, 1801968 (2018).
19. M. C. Scharber, D. Mühlbacher, M. Koppe, P. Denk, C. Waldauf, A. J. Heeger, and C. J. Brabec, *Adv. Mater.*, **18**, 789 (2006).